

## Local bond stress-slip behavior of reinforcing bars embedded in lightweight aggregate concrete

Chao-Wei Tang\*

Department of Civil Engineering & Geomatics, Cheng Shiu University, No. 840, Chengcing Rd.,  
Niaosong District, Kaohsiung City, Taiwan R.O.C.

(Received March 25, 2015, Revised August 6, 2015, Accepted August 18, 2015)

**Abstract.** This paper aims to study the local bond stress-slip behavior of reinforcing bars embedded in lightweight aggregate concrete (LWAC). The experimental variables of the local bond stress-slip tests include concrete strength (20, 40 and 60 MPa), deformed steel bar size (#4, #6 and #8) and coarse aggregate (normal weight aggregate, reservoir sludge lightweight aggregate and waterworks sludge lightweight aggregate). The test results show that the ultimate bond strength increased with the increase of concrete compressive strength. Moreover, the larger the rib height to the diameter ratio ( $h/d_b$ ) of the deformed steel bars is, the greater the ultimate bond stress is. In addition, the suggestion value of the CEB-FIP Model Code to the LWAC specimen's ultimate bond stress is more conservative than that of the normal weight concrete.

**Keywords:** lightweight aggregate concrete; bond mechanisms; pull-out test

---

### 1. Introduction

Bond failure of reinforced concrete (RC) members has been one of the major problems that may cause the collapse of structures under earthquake attack and is the primary objective of the study. In fact, the characteristic parameters for this complex problem have been suggested over the last few decades (Morohashi and Sakurada 2002, ACI Committee 408 2003, Ogura and Ichinose 2004, Zhu *et al.* 2004, Hossain *et al.* 2008, Ogura *et al.* 2008, Valcuende and Parra 2009, Desnerck *et al.* 2010, Hassan *et al.* 2010, Güneysisi *et al.* 2013, Alexandre *et al.* 2014, Aslani *et al.* 2014, Deng *et al.* 2014, Golafshani *et al.* 2014, Dehestani and Mousavi 2015, Mo *et al.* 2015, Zhou *et al.* 2015).

For normal-weight concrete (NWAC), most of the cracks are bond cracks at the aggregate-cement paste interface because the elastic modulus and strength of the aggregate are greater than those of the matrix, while for lightweight aggregate concrete (LWAC), the failure mechanism depends on whether the elastic modulus and strength of the lightweight aggregate (LWA) are greater than those of the matrix (Tang *et al.* 2009, Chen *et al.* 2011a, Chen *et al.* 2011b). Moreover, numerous studies dealing with mechanical properties have shown that significant differences exist between LWAC and NWAC (Husem 2003, Basche *et al.* 2007, ACI

---

\*Corresponding author, Professor, E-mail: [tangcw@gcloud.csu.edu.tw](mailto:tangcw@gcloud.csu.edu.tw)

Table 1 Physical properties of normal weight coarse/fine aggregate

Aggregate type	Specific weight (SSD)	Water absorption (SSD) (%)	Unit weight (dry-rodded) (kg/m <sup>3</sup> )	FM
Coarse aggregate	2.63	1.24	1532	-
Fine aggregate	2.56	1.33	-	2.75

Notes: SSD=Saturated surface dry condition; FM=Fineness modulus.

Committee 318 2008, Tang *et al.* 2009, Chen *et al.* 2011a, Chen *et al.* 2011b). To use the failure behavior of bond between concrete and deformed steel bar as an example, since there is a better bonding surface between the lightweight aggregate (LWA) and the cement paste in reinforced LWAC, and the elastic modulus values of these two materials are close and less than that of the NWAC, this delays the initial cracking during the transfer of bonding force. However, once the bar bond fails, breaking of LWAC will happen in the LWA with less strength. This situation is different from bond failure between the aggregate and the cement paste in NWAC. In other words, the flexural failure behavior of reinforced LWAC structural element will be different than that of the normal RC structural element. Thus, this paper aims to discuss the bond stress-slip relationship between deformed steel bar and LWAC.

For effectively getting the bond stress distribution in the major cracks after the flexural cracking of the RC structural element, the basic relationship equation of local bond stress-slip needs to be established. However, in fact, there are many factors which affect the local bond stress-slip relationship. Under the conditions of different rebar size, concrete strength and concrete aggregate type, this study performs the pull-out experiment to compare and analyze the effect of each factor and separately establish a local bond stress-slip formula. In addition, through regression analysis, the formula for the local ultimate bond stress between the deformed steel bar and the LWAC was presented.

## 2. Experimental program

### 2.1 Materials

Materials used for making specimens included cement, silica fume, fine and coarse aggregates, superplasticizer, and reinforcing steel. The cement used here was Type I Portland cement manufactured by Taiwan Cement Corporation with a specific gravity of 3.15 and a fineness of 3400 cm<sup>2</sup>/g. The silica fume was imported from Norway with a specific gravity of 2.08. The normal-weight coarse aggregate was crushed stone with a maximum particle size of 19 mm, and the fine aggregate was natural river sand. Their physical properties are listed in Table 1. In order to study the influence of LWA on the bond properties of concrete with various strength grades, two different types of synthetic LWA were used. One is made of fired reservoir sludge LWA (Type A), and the other is made of fired waterworks sludge LWA (Type B). The physical and mechanical properties of the two types of LWA are listed in Table 2 and Table 3, respectively. Two different superplasticizers (HICON HPC 1000 for medium strength concrete and HICON MTP A40 for high strength concrete) produced by Taiwan Jong Shin Company were used. Their physical properties are shown in Table 4. Three different reinforcing bars (#4, #6 and #8) of A706 were used. Their physical properties are shown in Table 5.

Table 2 Physical and mechanical of reservoir sludge LWA (Type A)

Sieve size	Percent retained (%)	Dry specific weight	Water absorption (%)		Crushing strength (MPa)
			30-min	24-hr	
1/2"-3/8"	64%	1.12	2.82	5.23	7.47
3/8"-4 <sup>#</sup>	36%	1.30	4.12	6.59	

Table 3 Physical and mechanical of waterworks sludge LWA (Type B)

Sieve size	Percent retained (%)	Dry specific weight	Water absorption (%)		Crushing strength (MPa)
			30-min	24-hr	
3/4"-1/2"	5.72	0.86	3.37	7.18	8.15
1/2"-3/8"	80.88	1.35	3.18	6.21	
3/8"-4 <sup>#</sup>	13.40	1.45	5.37	8.57	

Table 4 Basic properties of superplasticizer

Type	Specific weight	pH value	Solid composition (%)
HPC 1000	1.20	7±1	3.37
MTP A40	1.13	7±1	-

Table 5 Physical and mechanical of deformed bar

Bar No.	Nominal dia. (mm)	Nominal cross section area (cm <sup>2</sup> )	Rib distance (mm)	Rib width (mm)	Rib height (mm)	Elastic modulus (GPa)
4	12.70	1.27	8.3	2.1	0.7	204
6	19.05	2.85	12.1	3.7	1.9	207
8	25.40	5.07	30.4	3.7	1.7	205

Table 6 Mix proportions of LWAC (Type A)

Mix No.	W/B	Cement (kg/m <sup>3</sup> )	Silica fume (kg/m <sup>3</sup> )	Water (kg/m <sup>3</sup> )	FA (kg/m <sup>3</sup> )	LWA(kg/m <sup>3</sup> )		SP (kg/m <sup>3</sup> )	Dry unit weight (kg/m <sup>3</sup> )
						1/2"-3/8"	3/8"-4 <sup>#</sup>		
LA20	0.78	250	-	195	796	272	178	0	1546
LA40	0.48	394	-	189	665	279	182	1.38	1600
LA60	0.32	405	45	144	857	240	157	2.48	1740

Note: L=Lightweight aggregate concrete, A=Type A LWA, digits=Strength level, W/B=Water/binder ratio, SP=Superplasticizer (HICON HPC 1000 for LA40 and HICON MTP A40 for LA60).

Table 7 Mix proportions of LWAC (Type B)

Mix No.	W/B	Cement (kg/m <sup>3</sup> )	Silica fume (kg/m <sup>3</sup> )	Water (kg/m <sup>3</sup> )	FA (kg/m <sup>3</sup> )	LWA(kg/m <sup>3</sup> )		SP (kg/m <sup>3</sup> )	Dry unit weight (kg/m <sup>3</sup> )
						1/2"-3/8"	3/8"-4 <sup>#</sup>		
LB20	0.78	250	-	195	712	456	81	0	1570
LB40	0.48	394	-	189	671	429	76	1.38	1668
LB60	0.32	405	45	144	857	366	65	2.70	1790

Note: L=Lightweight aggregate concrete, B= Type B LWA, digits=Strength level, SP=Superplasticizer (HICON HPC 1000 for LB40 and HICON MTP A40 for LB60).

Table 8 Mix proportions of NWAC

Mix No.	Water/cement ratio (W/C)	Cement (kg/m <sup>3</sup> )	Water (kg/m <sup>3</sup> )	Aggregate(kg/m <sup>3</sup> )		SP (kg/m <sup>3</sup> )	Dry unit weight (kg/m <sup>3</sup> )
				FA	CA		
N20	0.76	267	203	772	1054	0	2147
N40	0.52	390	203	670	1054	0.78	2194
N60	0.32	591	189	523	1063	6.50	2301

Note: N=Normal weight aggregate concrete, digits=Strength level, FA=Fine aggregate, CA=Coarse aggregate, SP=Superplasticizer (HICON HPC 1000 for N40 and HICON MTP A40 for N60).

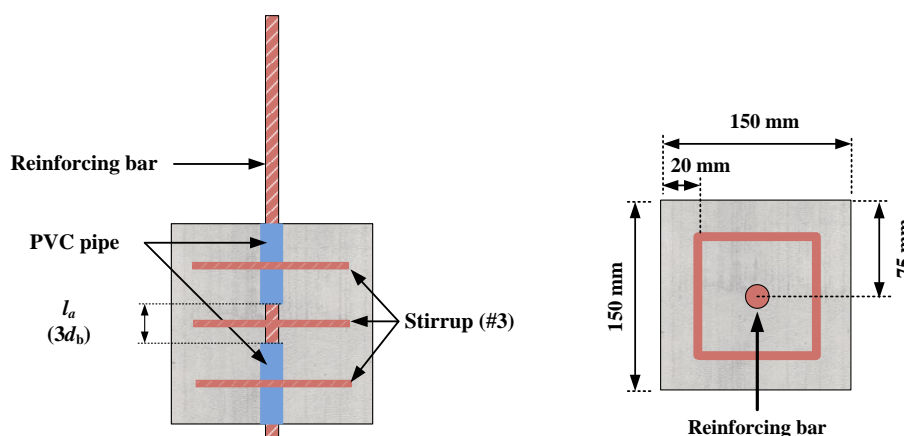


Fig. 1 Dimensions and cross-sections of specimen

## 2.2 Mix proportions and fabrication of specimens

Two types of concretes were made: LWAC and NWAC, the latter serving as the reference concrete. To analyze the influence of concrete strength on the bond behavior, the specified 28-day compressive strengths were chosen equal to 20, 40 and 60 MPa. The mix proportions for the LWAC are given in Tables 6-7. The mix proportions for the NWAC are given in Table 8. The abbreviations for identifying each concrete indicate the type of concrete – lightweight aggregate concrete (L) or normal-aggregate concrete (N) – the Type of LWA (A or B), and the strength of the concrete (20, 40 or 60 MPa).

All aggregates were cured in a room until the required saturated surface-dry condition was reached. The treated aggregates were then stored in a room in which the ambient temperature and relative humidity (RH) were controlled at  $25\pm 3^\circ\text{C}$  and  $50\pm 5\%$  to prevent moisture changes. In mixing, the cement (silica fume), fine aggregates, and coarse aggregates were generally blended first, and then water and superplasticizer were added. The mixing continued until a uniform concrete without any segregation was obtained.

Steel molds (150 mm cubic) were used to cast all the pullout specimens. The 150 mm cubic specimens with a single bar embedded vertically along the central axis were fabricated (see Fig. 1). The embedment lengths in the pullout specimens were determined to be three times the bar diameter (i.e.,  $l_a=3d_b$ ). This anchorage length, as suggested by Soroushian *et al.* (1994), is short enough to assume that the slippage recorded is representative of a local bond stress value. Those unbonded regions of the bar were sheathed with a PVC pipe. In addition, the specimens

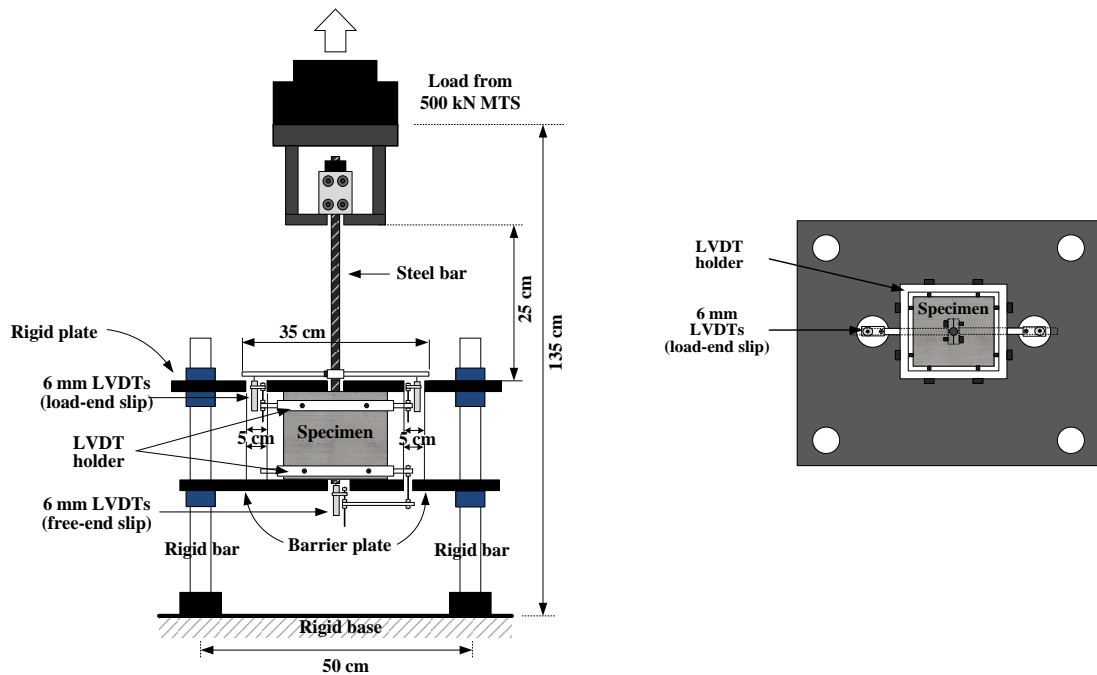


Fig. 2 Setup of pullout test

incorporate three transverse stirrups to limit splitting when the bar is placed in tension. Two nominally identical specimens were tested for each bar to check the reliability of the test setup and the scatter of the test results.

Freshly mixed concrete was slowly poured into the pullout specimen mold to a half depth across the horizontal surface and was followed by controlled vibrations. Immediately after the vibrations, the second half was poured in and was subjected to vibrations again to ensure that the concrete was well compacted. For each concrete mix, six 100-mm-diameter $\times$ 200-mm-high cylindrical specimens, referred to hereafter as control cylinders, were also cast. In addition, for each concrete mix, six 150-mm-diameter $\times$ 300-mm-high cylindrical specimens were also cast to determine the splitting tensile strength of concrete of given mix proportions. Following casting, all the specimens were covered overnight with a wet hessian and polyethylene sheets for a period of 24 hours. After 24 hours, the pullout specimens and their respective control cylinders were removed from the molds. To maintain the same environmental conditions, all specimens were placed in water containers in the laboratory for 27 days. After curing the specimens were removed from water.

### 2.3 Instrumentation and test procedures

The pullout specimens were conducted using a 500 kN MTS servo valve controlled machine equipped with a specially fabricated testing frame as shown in Fig. 2. The linear variable differential transformers (LVDT) were used to measure relative bond slip between the bar and the concrete at the loaded as well as the free ends; the detailed test setup is shown in Fig. 2. The pullout force was applied at a constant displacement rate of 0.01 mm/sec up to bond failure. The

Table 9 Mechanical properties of concrete

Mix No.	Compressive strength (MPa)	Splitting strength (MPa)	Elastic modulus (GPa)
N20	20.20	2.40	23.32
N40	40.97	2.91	30.22
N60	59.46	3.23	30.72
LA20	20.35	1.65	16.40
LA40	40.50	2.03	21.58
LA60	58.39	5.15	26.73
LB20	21.14	1.79	24.12
LB40	39.96	2.53	26.01
LB60	57.57	4.68	29.74

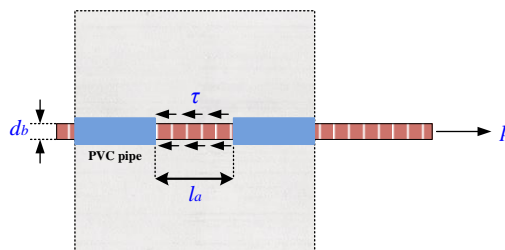


Fig. 3 Schematic diagram of local bond stress between bar and concrete

pullout force was measured by a load cell fitted in the testing machine. The test progress was monitored on a computer screen, and all load and displacement data were captured and stored in a diskette via a data logger.

### 3. Experimental results and discussion

#### 3.1 Mechanical properties of concrete

On the day of the pullout test, the respective control cylinders were capped and tested in compression to determine the compressive strength of concrete. Mean compressive strength was calculated by taking average of three specimens. Table 9 shows that the average values of 28-day compressive strengths are close to the target values (i.e. 20, 40 and 60 MPa). In addition, Table 9 also shows the average values of the splitting tensile strength and elastic modulus for the NWAC and the LWAC.

#### 3.2 Local bond stress-slip behavior

During the loading of the pullout test, load is transferred between the bar and the surrounding concrete through adhesion and mechanical bond. The mechanical bond is provided by the bar lugs bearing against the surrounding concrete. This is the dominant load transfer mechanism, with its strength limit state typically controlled by splitting of the surrounding concrete (Ogura et al. 2008). Assuming that the bond stresses are uniformly distributed along the bonded length (see Fig. 3), the

bond stress can be calculated by dividing the measured force by the bonded surface area of the deformed steel bar, as shown in the following equation

$$\tau = \frac{P}{\pi d_b l_a} \quad (1)$$

where  $\tau$ =bond stress (MPa);  $P$ =pullout force (N);  $d_b$ =bar diameter (mm);  $l_a$ =bond length (mm).

By measuring the force applied to the ribbed bar and the displacement of the bar in relation to the concrete surface, a bond stress-slip relation can be determined. The relative slip of the deformed bar and the concrete corresponding to the bond stress can be divided into the loading end slip  $s_l$  and the free end slip  $s_f$ . In the condition of local bond, the relative slip of bar and concrete can be treated as rigid motion, thus the  $s_l$  and  $s_f$  should be the same under the same loading. In this study, take the average of  $s_l$  and  $s_f$  as the slip corresponding to bond stress, as shown in the following equation

$$s = \frac{s_l + s_f}{2} \quad (2)$$

Overall, the global behavior of the bond stress-slip relationship for the test specimens is characterized by an initial increase in the bond stress with little slippage, which is then followed by softening once the maximum bond stress is attained. The local bond stress-slip curves for specimens with different concretes and bar numbers are presented in Figs. 4-6. The bond stress-slip curves were deduced by taking force value at a given slip value and converting into bond stress using Eq. (1). From the pullout test results, it can be seen that the local bond stress-slip curve can be divided into five stages (see Fig. 7), as described below:

- Non-slip phase: In the initial period of loading, because of the chemical bonding force between bar and matrix, there is a short non-slip straight line section.
- Slight slip phase: When the loading is up to  $\tau_1/\tau_u \approx 0.3$ , the chemical bonding force between bar and matrix fails, and the bar and concrete start to produce a relative slip.
- Splitting phase: When the loading increases continually and the bond stress reaches splitting bond stress ( $\tau_{cr}$ ), radial splits appear around the bar due to radial pressure exerted by the bar lugs. The confining effect of the stirrup, however, can delay the development of splitting and loading can steadily increase.
- Decreasing phase: When the loading is increased continually to the ultimate bond stress ( $\tau_u$ ), the concrete within the net gap between bar ribs is crushed completely, and shear-cut slip along the rib O.D. occurs. At this time, the bond stress decreases quickly and the slip amount increases quickly.
- Residual phase: When the slip amount reaches  $s_3$ , approximately one bar rib-net spacing, the concrete between ribs is completely cut-off. At this time, the bond stress decreases no more. Only the frictional force between the bar and the surrounding concrete provides residual bond stress ( $\tau_f$ ).

### 3.3 Failure modes

In general, there are two recognized modes of bond failure, i.e., splitting failure and pullout failure. In the study, most of the tested specimens failed in pullout mode, while a few specimens failed in splitting failure mode. As shown in Figs. 4-6, bond stress-slip curves are initially very

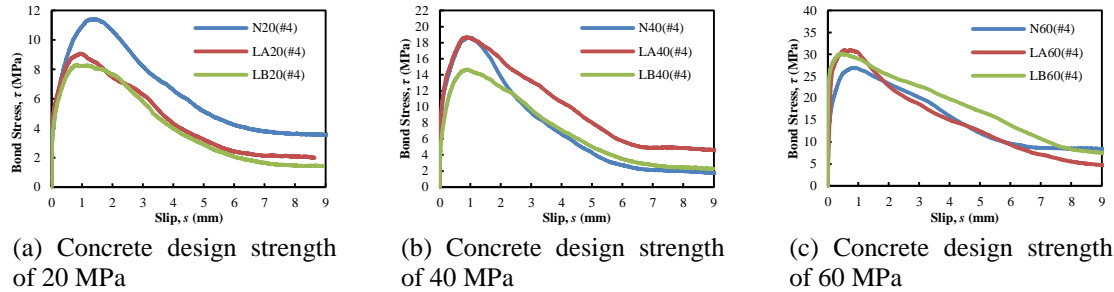


Fig. 4 Local bond stress-slip curve for specimens with #4 bar

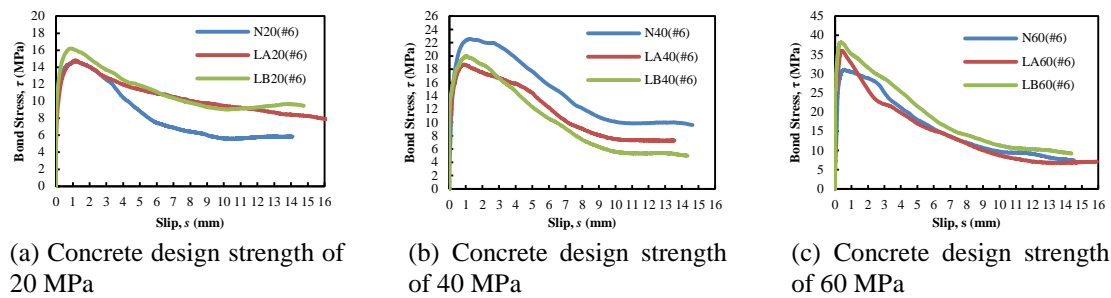


Fig. 5 Local bond stress-slip curve for specimens with #6 bar

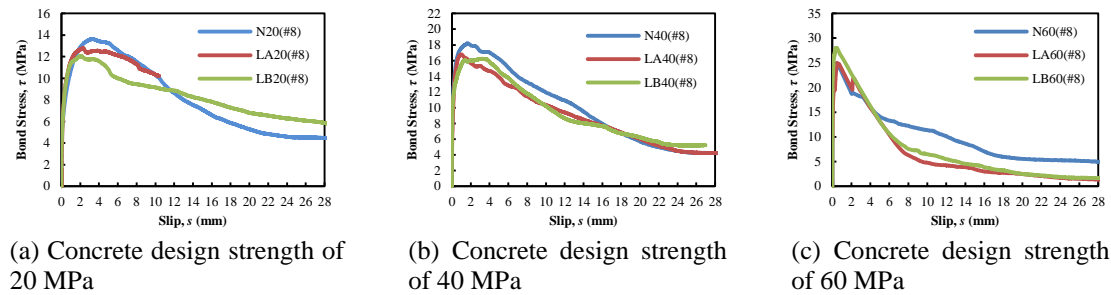


Fig. 6 Local bond stress-slip curve for specimens with #8 bar

step because of adhesion. In addition, the bond stress magnitude did vary depending on the variables being tested, most notably the reinforcing bar size. No matter what the concrete strength level, all specimens with #4 bar exhibited pullout failure. It is characterized by an increasing amount of slip until the bar pulls out of the concrete and the bond strength lessens considerably.

Table 9 shows that as the compressive strength of concrete increases, its splitting strength also increases. Thus, along with the increase in compressive strength, the bond performance between the bar and the concrete also increases, developing higher bond stress before failure. As the bond stress reaches the splitting strength of the concrete, the concrete around the deformed bars produces radial split. This kind of split originates from the wedging action of the reinforcing steel rib and develops along the bar radial direction to the specimen surface. After the production of split, the stress on the stirrup suddenly increases. Since the confinement of the stirrup restricts the development of split, the bond stress slightly rise up. At this moment, the bar slips greatly.

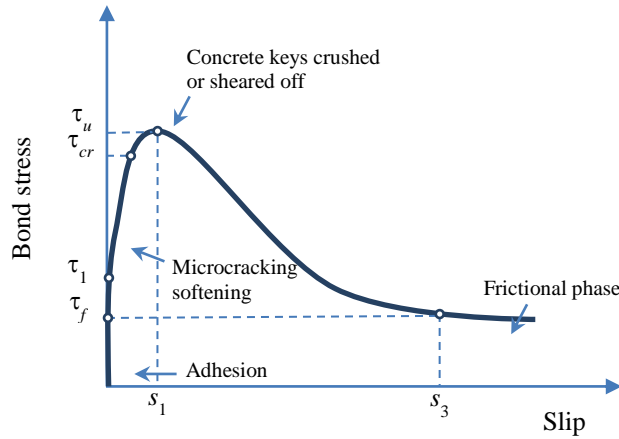


Fig. 7 Typical local bond stress-slip curve

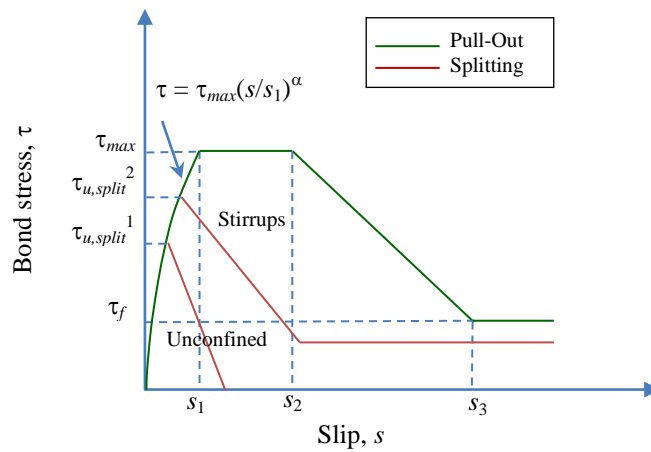


Fig. 8 Analytical bond stress-slip relationship (CEB-FIP Model Code 2010)

For high strength concrete (60 MPa) specimens with #6 bar and #8 bar, the concrete cover is less than that of the #4 bar, and under the condition of embedment length equivalent to  $3d_b$ , its embedment length of rebar is longer than that of the #4 bar specimen. Therefore, when the bond stress develops to a fixed level, since the stirrup cannot bear the giant radial drawing stress, the split continues to extend to the concrete surface. This causes failure as a result of split before developing to a real ultimate bond stress. As can be seen from Fig. 5 and Fig. 6, bond stress decreased dramatically when the specimens produce splitting failure. This makes bar and concrete lose its bond performance. As a result, only the frictional force between the bar and the surrounding concrete can provide residual bond stress.

The nonlinear bond stress-slip relation recommended by the CEB-FIP Model Code 2010 (Fig. 8) is employed. Therefore, the bond stress ( $\tau$ ) between concrete and bar can be calculated as a function of the relative displacement ( $s$ ) according to Eqs. (3)-(6)

$$\tau = \tau_{max} \left( \frac{s}{s_1} \right)^\alpha \quad \text{for } 0 \leq s \leq s_1 \quad (3)$$

$$\tau = \tau_{max} \quad \text{for } s_1 < s \leq s_2 \quad (4)$$

$$\tau = \tau_{max} - (\tau_{max} - \tau_f) \left( \frac{s - s_2}{s_3 - s_2} \right) \quad \text{for } s_2 < s \leq s_3 \quad (5)$$

$$\tau = \tau_f \quad \text{for } s_3 < s \quad (6)$$

where  $\tau_{max}$  is the peak bond stress;  $\tau_f$  is the residual bond stress,  $s$  is the bond slip; and  $s_1$ ,  $s_2$  and  $s_3$  are the slip at the start of peak bond stress, slip at the end of peak bond stress and slip at the start of residual bond stress, respectively.

The parameters in the CEB-FIP Model have been prescribed in the code for confined and unconfined normal strength concrete with good or other bond conditions. Therefore, the CEB-FIP Model Code is compared with the measured bond stress-slip behavior of the specimen (see Figs. 9-10). From these figures, it can be seen that the predicted values calculated with the CEB-FIP Model Code for high strength concrete underestimated the bond strength in all specimens with #4 bar and #6 bar. In addition, it can be seen that the bond stress-slip relation for the NWAC specimens is closer to the CEB-FIP Model Code specified curve than those for the LWAC specimens. On the other hand, the slope of the curve for all specimens is far greater than those specified in the CEB-FIP Model. This means that under the same bond stress, the measured slip is smaller than the value specified in the CEB-FIP Model Code. But compared to NWAC, there is an evident difference between the LWAC and the CEB-FIP Model.

Theoretically, residual bond stress is associated with ultimate bond. Therefore, when there is some difference between the ultimate bond stress and the predicted values calculated with the CEB-FIP Model Code, the residual bond stress will also have some differences. As to the value of slip at the start of residual bond stress, either NWAC or LWAC is close to the suggested value by the CEB-FIP Model Code, which is equal to one bar rib-net spacing.

From the comparison of experimental results of the two LWAC specimens made of LWAs with different raw materials, that their local bond stress-slip relationship curves are similar. It can be seen from Tables 2-3 that the crushing strengths of the reservoir sludge lightweight aggregate and the waterworks sludge light-weight aggregate are 7.47 MPa and 8.15 MPa, respectively. The difference of crushing strength between the two LWA is not evident. From this viewpoint, when the LWA mechanical properties are close, their local bond stress-slip behavior is similar. In other words, the coarse aggregate type of concrete has a certain effect on the local bond stress-slip behavior of reinforced concrete members.

### 3.4 Ultimate bond stress

For RC members, when the bond stress between the concrete and the ribbed bar reaches the maximum allowed value, the ribbed bar and the concrete will lose the ability to jointly resist external force. Basically, bond properties can be revealed as good or bad by comparing the ultimate bond stress ( $\tau_u$ ) of the specimens. Especially under the condition of local bond, the effect of uneven distribution bar embedment length on bond stress can be excluded. In other words, the comparative result of local bond tests is more representative. Table 10 presents the experimental

Table 10 Comparison of ultimate bond stress between test result and CEB-FIP Model

Specimen No.	Ultimate bond stress $\tau_u$ (MPa)			CEB-FIP Model	Difference percentage (%)
	Experiment results				
	Specimen1	Specimen2	Average		
N20(#4)	12.52	11.42	11.18		-6.60
N20(#6)	14.71	14.42	14.57	11.97( $\tau_u=2.5f_c^{0.5}$ )	21.72
N20(#8)	13.58	13.63	13.61		13.66
N40(#4)	16.30	18.61	17.46		10.40
N40(#6)	23.64	22.57	22.92	15.81( $\tau_u=2.5f_c^{0.5}$ )	46.14
N40(#8)	19.14	18.20	18.67		18.09
N60(#4)	30.55	26.88	28.72		48.32
N60(#6)	31.04	31.79	31.41	19.36( $\tau_u=2.5f_c^{0.5}$ )	62.27
N60(#8)	24.35	26.68	25.52		31.79
LA20(#4)	10.75	9.08	9.91		41.64
LA20(#6)	16.53	14.79	15.66	7.00( $\tau_u=0.6f_c^{0.82}$ )	123.71
LA20(#8)	12.77	12.97	12.87		83.86
LA40(#4)	18.65	17.14	17.90		44.90
LA40(#6)	20.41	18.72	19.57	12.35( $\tau_u=0.6f_c^{0.82}$ )	58.42
LA40(#8)	14.80	16.78	15.79		27.85
LA60(#4)	31.00	28.81	29.90		73.56
LA60(#6)	35.97	33.65	34.81	17.23( $\tau_u=0.6f_c^{0.82}$ )	102.03
LA60(#8)	22.5	24.94	23.71		37.67
LB20(#4)	11.15	8.32	9.73		39.07
LB20(#6)	14.98	16.20	15.59	7.00( $\tau_u=0.6f_c^{0.82}$ )	122.71
LB20(#8)	11.83	12.03	11.93		70.43
LB40(#4)	16.33	14.64	15.49		25.38
LB40(#6)	23.67	19.98	21.82	12.35( $\tau_u=0.6f_c^{0.82}$ )	76.72
LB40(#8)	16.23	16.39	16.31		32.06
LB60(#4)	30.96	30.08	30.52		77.13
LB60(#6)	38.13	40.01	39.07	17.23( $\tau_u=0.6f_c^{0.82}$ )	126.76
LB60(#8)	28.00	24.75	26.38		53.08

results of ultimate bond stress for each specimen.

### 3.4.1 Comparison with CEB-FIP Model Code

For specimens with good confinement and non-split failure, the local  $\tau$ - $s$  relationship curves suggested by the CEB/FIP Model Code (1990, 2010) were used to calculate the values of  $\tau_u$ , as shown in the following equations

$$\text{NWAC: } \tau_u = 2.5f_c^{0.5} \text{ (Unit: MPa)} \tag{7}$$

$$\text{LWAC: } \tau_u = 0.6f_c^{0.82} \text{ (Unit: MPa)} \tag{8}$$

where  $f_c'$  is the concrete compressive strength. From Eq. (7) and Eq. (8), it can be seen that for the

Table 11 Bond Modulus for specimens with various bar diameters

Mix No.	Bond Modulus, $\kappa (\tau/0.4s_1)$		
	#4 bar	#6 bar	#8 bar
N20	18.9	24.7	8.8
N40	35.5	40.3	25.3
N60	72.5	119.6	53.5
LA20	20.2	29.4	15.1
LA40	37.2	46.2	39.4
LA60	126.5	162.2	77.8
LB20	19.6	40.2	13.1
LB40	30.3	44.1	38.3
LB60	169.2	159.1	99.6

calculation of the ultimate bond stress, the CEB/FIP Model Code only consider the effect of concrete compressive strength, and did not consider other factors.

The experimental results of  $\tau_u$  for each specimen together with their suggested magnitude by the CEB/FIP Model Code are compiled in Table 10. As can be seen from Table 10, no matter what the concrete strength level or bar size, the difference between the measured  $\tau_u$  and the recommended  $\tau_u$  by the CEB/FIP Model Code for the LWAC was far greater than for the NWAC. The difference for the NWAC can reach 62%, while the difference for the LWAC up to about 127%. These results indicate that the recommended  $\tau_u$  by the CEB/FIP Model Code for the LWAC is more conservative than for the NWAC. On the other hand, under the same conditions of the concrete strength, regardless of the types of concrete, the experimental results of  $\tau_u$  varied with the bar size. In addition, the maximum difference between the measured  $\tau_u$  and the recommended  $\tau_u$  by the CEB/FIP Model Code is in specimens with #6, no matter what the type and strength level of concrete. Therefore, the effect of size on  $\tau_u$  is quite significant. Moreover, with the increasing strength level of concrete, the difference between the measured  $\tau_u$  and the recommended  $\tau_u$  by the CEB/FIP Model Code is more obvious. Summing up the above results, the influence of the bar size on  $\tau_u$  is quite important. Therefore, the CEB/FIP Model Code only considering the effect of concrete strength on  $\tau_u$  is insufficient to accurately estimate the test results.

#### 3.4.2 Effect of bar size on ultimate bond stress

In exploring the bond performance between concrete and bar, the diameter of the deformed steel bars also plays a very critical role. Theoretically, the rib area increases with increasing bar diameter. However, the shape parameter does not follow a linear change; the rib height is relatively lower. Accordingly, the actual increase in the rib area is insignificant. In other words, the larger the diameter of the bar, the bond area is relatively smaller. As a result,  $\tau_u$  is smaller.

Figs. 11-12 show that under the same condition of the concrete strength or the type of coarse aggregate, the  $\tau_u$  of specimens with #4 and #8 are lower than that of specimens with #6. The reason is the  $\tau_u$  of specimens is significantly related to the rib height of bar. It can be seen from Table 5 that the values of rib height for #4, #6 and #8 are 0.7 mm, 1.9 mm and 1.7 mm, respectively.

On the other hand, the rib height to the diameter ratio ( $h/d_b$ ) of the deformed steel bars can be used as a parameter to explore its effect on  $\tau_u$ . According to the physical properties of steel used in this study (see Table 5), the values of  $h/d_b$  for #4, #6 and #8 are 0.055, 0.1 and 0.067, respectively. It can be seen from Fig. 13 that for specimens failed in pullout mode, the greater the value of  $h/d_b$ ,

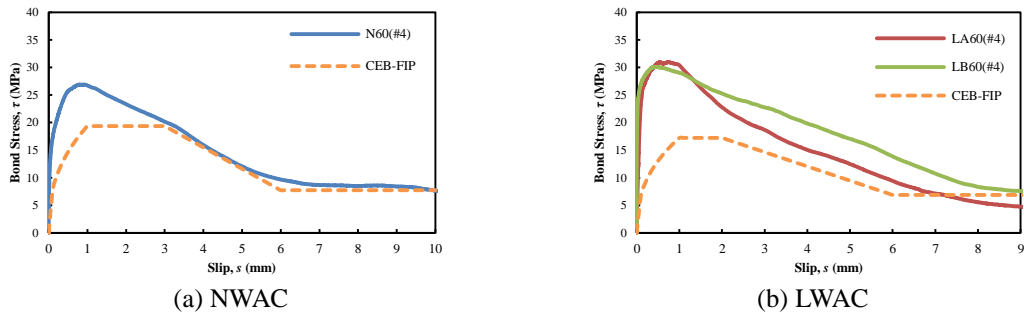


Fig. 9 Comparison of local bond stress-slip curve with CEB-FIP (for specimens with #4 bar)

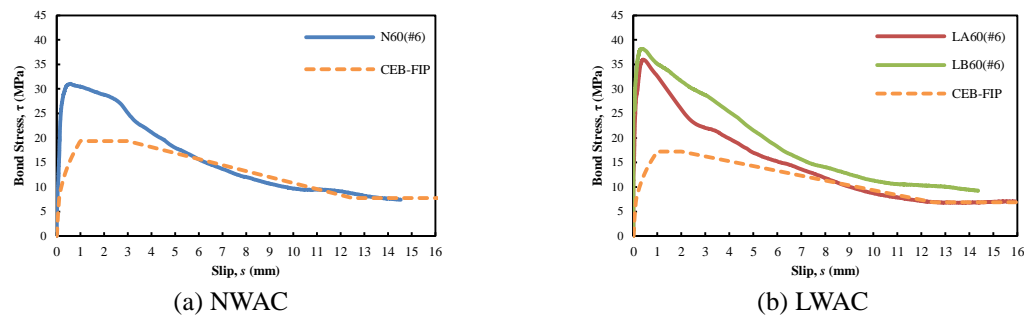


Fig. 10 Comparison of local bond stress-slip curve with CEB-FIP (for specimens with #6 bar)

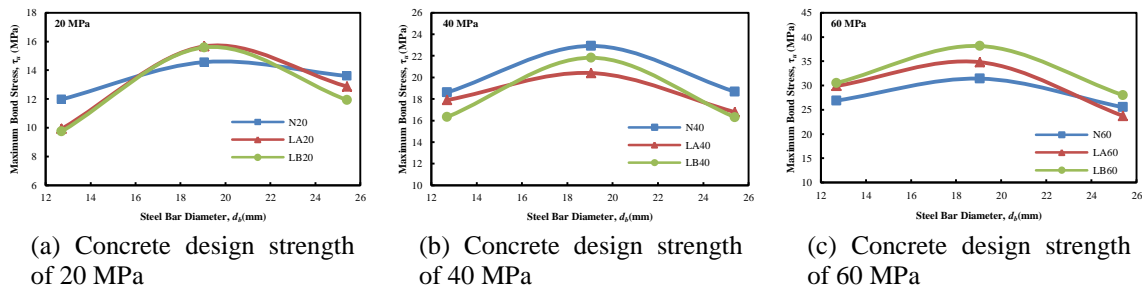


Fig. 11 Relationship between bar diameter and ultimate bond stress for various strengths of concrete

is, the greater the  $\tau_u$  is. From this perspective, the use of  $h/d_b$  in analyzing  $\tau_u$  not only demonstrates a regular linear relationship but also interprets test results well.

### 3.4.3 Effect of concrete strength and coarse aggregate type on ultimate bond stress

Fig. 11 shows that the measured  $\tau_u$  increased with increasing concrete strength. Under the condition of low concrete strength (20 MPa), the values of measured  $\tau_u$  for the LWAC specimens were slightly lower than for the NWAC; under the condition of medium concrete strength (40 MPa), the values of measured  $\tau_u$  for the LWAC specimens were similar to those of the NWAC; while under the condition of high concrete strength (60 MPa), the values of measured  $\tau_u$  for the LWAC specimens were significantly higher than for the NWAC. The results showed that the  $\tau_u$  of high strength LWAC was no worse than that of the NWAC with the same strength level, or even

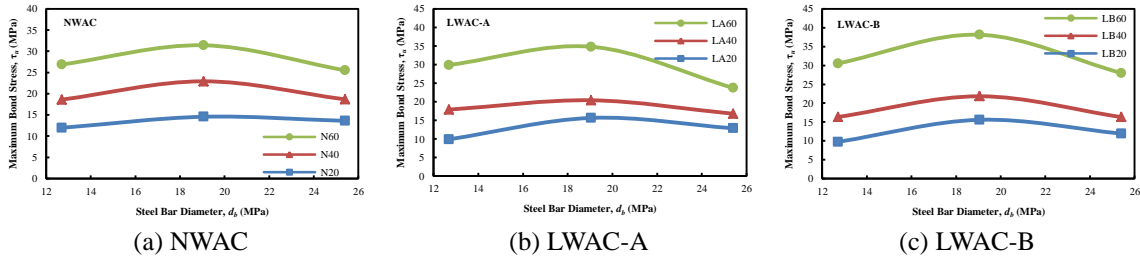


Fig. 12 Relationship between bar diameter and ultimate bond stress for various types of concrete

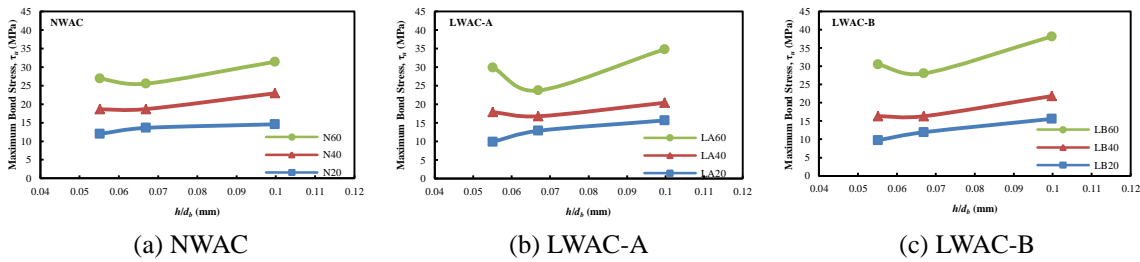


Fig. 13 Relationship between bar rib height-diameter ratio value and ultimate bond stress

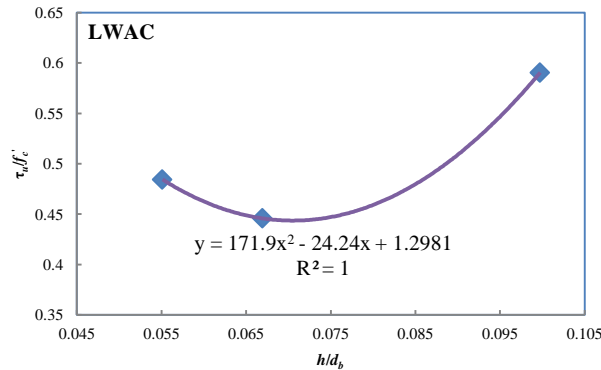


Fig. 14 Empirical formula for local ultimate bond stress

better than NWAC. This is relevant to the bearing characteristic of the LWAC and NWAC.

In general, regardless of the strength level of LWAC, the strength of LWA is often lower than the strength of the cement mortar in LWAC, resulting in inferior bearing characteristic. Therefore, once the bar bond fails, breaking of LWAC will usually happen in the LWA. In other words, the mortar matrix is the main factor affecting bond fail in LWAC. By contrast, the failure mechanism in NWAC is very different. Under the condition of lower concrete strength, the normal weight aggregate in the cracked surface is mostly unspoiled, which is able to provide a higher bearing characteristic, thus enhancing the overall bond strength. But under the condition of high strength concrete, the failure mechanism in the NWAC is similar to the LWAC. In other words, regardless of normal weight aggregate or lightweight aggregate, the aggregate in the cracked surface is often cleaved or broken. The bearing force provided by aggregates is relatively small, thus the mortar matrix is the main factor affecting bond fail in both the LWAC and NWAC. While under the same

condition of concrete strength level, the cement mortar strength of the LWAC is higher than that of the NWAC. Therefore, under the condition of higher concrete strength (60 MPa), the cement mortar of the LWAC can provide better support force, resulting in the bond strength is better than that of the NWAC.

#### 3.4.4 Empirical formula of ultimate bond stress

The foregoing show that the CEB-FIP model Code is inappropriate for the predicting bond stress-slip behavior of steel bars embedded in high strength LWAC. Therefore, this paper proposes an empirical formula of ultimate bond stress to take in to account the effect of the bar diameter.

Under the same condition of experimental parameters, the ultimate bond stress for the two types of LWAC is very close. Therefore, the experimental data for the two types of LWAC were gathered together and analyzed. The relationship between the rib height to the diameter ratio ( $h/d_b$ ) of the deformed steel bars and the ultimate bond stress to the concrete compressive strength ratio ( $\tau_u/f_c'$ ) was established to obtain the regression equation and the coefficient of determination ( $R^2$ ) (see Fig. 14). The established empirical formula for local ultimate bond stress is shown below

$$\tau_u = \left[ 171.9 \left( \frac{h}{d_b} \right)^2 - 24.24 \left( \frac{h}{d_b} \right) + 1.2981 \right] f_c' \quad (9)$$

According to the established empirical formula, the calculated values of  $\tau_u$  were compared with the experimental value. Fig. 14 shows that the empirical formula fits well with the experimental values. Therefore, the established empirical formula for local ultimate bond stress is suitable for the LWAC specimens with similar bond conditions and has certain accuracy.

### 3.5 Local slip

In the local bond stress-slip model proposed by the CEB/FIP Model Code, the bond stress-slip curve is initially very steep (see Fig. 8). Especially, the bond stress-slip relationship is more nonlinear near the ultimate bond stress. Before the stress reaches the ultimate value, the splitting cracks in the concrete will also cause an impact on slip. In other words, only by comparing slip  $s_1$ , it is difficult to have good and accurate results. In view of this, it is assumed that the bond stress-slip relationship is linear when the slip value is between zero and  $0.4s_1$ , as shown in the following equation

$$\tau(s) = \kappa \cdot s(x) \quad (10)$$

where,  $\tau(s)$ =local bond stress (only a function of the relative slip);  $s(x)$ =relative slip;  $\kappa$ =bond modulus (the paper takes  $\kappa=\tau/0.4s_1$ ). In fact, the bond modulus has its physical meaning. If the bond stress maintains a certain value, the greater the value of the bond modulus is, the smaller the slip. Therefore, under each variable fixed condition, through the applications of  $\kappa$  to compare the differences between the bond stress-slip relationships, the result will be clearer.

Under the same condition of concrete aggregate type, the effect of concrete compressive strength on the bond modulus is shown in Table 11. It can be seen from Table 11 that the bond modulus increased with increasing concrete strength. The reason is the bond characteristic between bar and concrete becomes better owing to the increase of the concrete strength, so the relative slip between the concrete and the bar is also smaller. As can be seen from Fig. 15, under the concrete

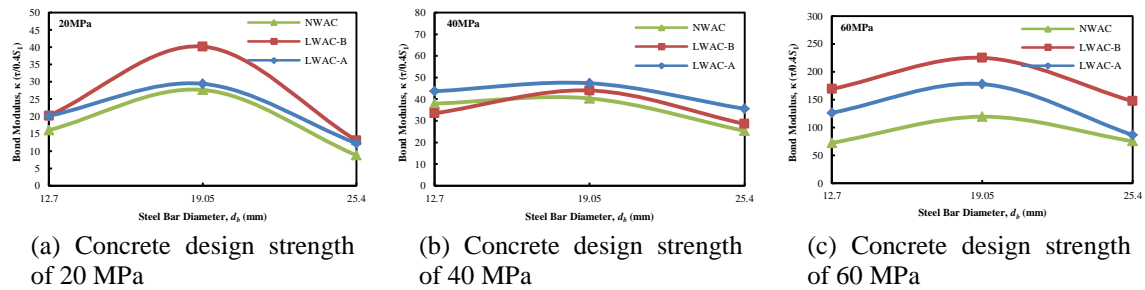


Fig. 15 Comparison of bond modulus under the same concrete compressive strength

strength fixed condition, the bond modulus of specimens with #6 is the maximum and the bond modulus of specimens with #8 is the minimum, while the bond modulus of specimens with #4 is somewhere between minimum and maximum. This is because the rib height of #4 is relatively lower. In view of this, in order to ensure objective results, the percentage of the rib area to the overall bond area should be considered.

It can also be seen from Fig. 15, with the bar size from #6 to #8, the attenuation amplitude of the bond modulus for specimens with high-strength concrete (60 MPa) is far greater when compared with low- and medium-strength concrete. This result shows that under the same bond stress, the value of slip for specimens with #8 would be much higher than for specimens with #6. In other words, the bond slip behavior of high-strength RC members with tension cracking will vary quite significantly, depending on the bar size.

On the other hand, Fig. 15 shows that under the same condition of concrete strength, regardless of the bar diameter, the bond modulus for the LWAC specimens is mostly higher than that of the NWAC specimens; especially for high strength concrete (60 MPa). It can be noted that under the same condition of local bond stress, the values of slip for the LWAC specimens were lower than for the NWAC specimens; or under the same condition of slip, the local bond stress for the LWAC specimens were higher than for the NWAC specimens. This is contrary to the general idea that under the same condition of concrete strength, the elastic modulus of for the LWAC specimens was lower than for the NWAC specimens, resulting in its axial deformation is relatively higher under the same axial stress. The reason is the effect of the embedment length of bar on the internal force and deformation of the specimen has been reduced in the local bond-slip test. The relative slip between bar and concrete is a rigid body motion, resulting in the bond stress has little effect on the strain of the overall concrete. In the specimens, the steel surface is mainly coated by cement mortar, which is the main factor to influence the relative slid between the bar and the concrete; the higher the strength of cement mortar is, the higher the stiffness (i.e., per unit length can have a greater ability to resist deformation). While under the same condition of concrete strength, the cement mortar strength of the LWAC is higher than that of the NWAC. Therefore, under the same condition of local bond stress, the value of slip for the LWAC is relatively lower than that of the NWAC.

#### 4. Conclusions

The local bond stress-slip behavior of LWAC specimens were described and compared with

companion NWAC specimens. The influences of material parameters were thoroughly analyzed. Based on the experimental results, the following conclusions can be drawn:

1. Under the same condition of bar size, the ultimate bond stress of the LWAC specimens with middle/low strengths is slightly lower than that of the NWAC specimens. However, the ultimate bond stress of the LWAC specimens with high strength is obviously higher than that of the NWAC specimens.
2. The ultimate bond strength increased with the concrete compressive strength. Moreover, the larger the rib height to the diameter ratio ( $h/d_b$ ) of the deformed steel bars is, the greater the ultimate bond stress is.
3. The CEB-FIP Model Code does not implement the influence of the bar diameter and is quite conservative in predicting the ultimate bond strength for both the LWAC and the NWAC specimens with high strength level. Moreover, the suggestion value of the CEB-FIP Model Code to the LWAC specimen's ultimate bond stress is more conservative than that of the NWAC.
4. The established empirical formula for local ultimate bond stress is a function of concrete strength and  $h/d_b$ , which fits well with the experimental values.

## Acknowledgments

The author expresses his gratitude and sincere appreciation to the Ministry of Science and Technology, Taiwan, for financing this research work.

## References

- ACI Committee 408 (2003), *Bond and Development of Straight Reinforcing Bars in Tension (ACI 408R-03)*, American Concrete Institute, Farmington Hills, Mich.
- ACI Committee 318 (2011), *Building Code Requirements for Structural Concrete (ACI 318-11) and Commentary*, American Concrete Institute, Farmington Hills, Mich.
- Alexandre Bogas, J., Gomes, M.G. and Real, S. (2014), "Bonding of steel reinforcement in structural expanded clay lightweight aggregate concrete: The influence of failure mechanism and concrete composition", *Constr. Build. Mater.*, **65**, 350-359.
- Aslani, F., Nejadi, S. and Samali, B. (2014), "Short term bond shear stress and cracking control of reinforced self-compacting concrete one way slabs under flexural loading", *Comput. Concrete*, **13**(6), 709-737.
- Basche, H.D., Rhee, I., Willam, K.J. and Shing, P.B. (2007), "Analysis of shear capacity of lightweight concrete beams", *Eng. Fract. Mech.*, **74**(1-2), 179-193.
- CEB (1992), *CEB-FIP Model Code 90*, Thomas Telford, London, UK.
- CEB (2010), *CEB-FIP Model Code 2010*, Lausanne, Switzerland.
- Chen, H.J., Tsai, W.P., Tang, C.W. and Liu, T.H. (2011), "Time-dependent properties of lightweight concrete using sedimentary lightweight aggregate and its application in prestressed concrete beams", *Struct. Eng. Mech.*, **39**(6), 833-847.
- Chen, H.J., Liu, T.H., Tang, C.W. and Tsai, W.P. (2011), "Influence of high-cycle fatigue on the tension stiffening behavior of flexural reinforced lightweight aggregate concrete beams", *Struct. Eng. Mech.*, **40**(6), 847-866.
- Dehestani, M. and Mousavi, S.S. (2015), "Modified steel bar model incorporating bond-slip effects for embedded element method", *Constr. Build. Mater.*, **81**, 284-290.
- Deng, Z.C., Jumbe, R.D. and Yuan, C.X. (2014), "Bonding between high strength rebar and reactive powder

- concrete”, *Comput. Concrete*, **13**(3), 411-421.
- Desnerck, P., De Schutter, G. and Taerwe, L. (2010), “Bond behaviour of reinforcing bars in self-compacting concrete: experimental determination by using beam tests”, *Mater. Struct.*, **43**(1), 53-62.
- Golafshani, E.M., Alireza Rahai, A. and Kebria, S.S.H. (2014), “Prediction of the bond strength of ribbed steel bars in concrete based on genetic programming”, *Comput. Concrete*, **14**(3), 327-359.
- Güneyisi, E., Gesoğlu, M. and Ipek, S. (2013), “Effect of steel fiber addition and aspect ratio on bond strength of cold-bonded fly ash lightweight aggregate concretes”, *Constr. Build. Mater.*, **47**, 358-365.
- Hassan, A.A.A., Hossain, K.M.A. and Lachemi, M. (2010), “Bond strength of deformed bars in large reinforced concrete members cast with industrial self-consolidating concrete mixture”, *Constr. Build. Mater.*, **24**(4), 520-530.
- Hossain, K.M.A. and Lachemi, M. (2008), “Bond behavior of selfconsolidating concrete with mineral and chemical admixtures”, *J. Mater. Civil Eng.*, ASCE, **20**(9), 608-616.
- Husem, M. (2003), “The effects of bond strengths between lightweight and ordinary aggregate-mortar, aggregate-cement paste on the mechanical properties of concrete”, *Mater. Sci. Eng. A*, **363**, 152-158.
- Mo, K.H., Alengaram, U.J., Visintin, P., Goh, S.H. and Jumaat, M.Z. (2015), “Influence of lightweight aggregate on the bond properties of concrete with various strength grades”, *Constr. Build. Mater.*, **84**, 377-386.
- Morohashi, N. and Sakurada, T. (2002), “Effect of concrete strength on bond splitting strength of lap splice”, *JCI Ann. J.*, **24**(2), 787-92.
- Ogura, N. and Ichinose, T. (2004), “Analytical study on splitting bond failure of deformed bars”, *AII J. Struct. Constr. Eng.*, **586**, 147-153.
- Ogura, N., Bolander, J.E. and Ichinose, T. (2008), “Analysis of bond splitting failure of deformed bars within structural concrete”, *Eng. Struct.*, **30**(2), 428-435.
- Soroushian, P., Mirza, F. and Alhozaimy, A. (1994), “Bonding of confined steel fiber reinforced concrete to deformed bars”, *ACI Mater. J.*, **91**(2), 144-149.
- Tang, C.W., Yen, T. and Chen, H.J. (2009), “Shear behavior of reinforced concrete beams made with sedimentary lightweight aggregate without shear reinforcement”, *J. Mater. Civil Eng.*, ASCE, **21**(12), 730-739.
- Valcuende, M. and Parra, C. (2009), “Bond behaviour of reinforcement in self-compacting concretes”, *Constr. Build. Mater.*, **23**(1), 162-170.
- Zhou, H., Lu, J., Xu, X., Dong, B. and Xing, F. (2015), “Effects of stirrup corrosion on bond-slip performance of reinforcing steel in concrete: An experimental study”, *Constr. Build. Mater.*, **93**, 257-266.
- Zhu, W., Sonebi, M. and Bartos, P.J.M. (2004), “Bond and interfacial properties of reinforcement in self-compacting concrete”, *Mater. Struct.*, **37**, 442-448.